Graph-based Segmentation of Optimal IVUS Media-Adventitia Border using Shape Prior

Ehab Essa[1]
csehab@swansea.ac.uk
Xianghua Xie[1]
X.Xie@swansea.ac.uk
Igor Sazonov[2]
I.Sazonov@swansea.ac.uk
Perumal Nithiarasu[2]
P.Nithiarasu@swansea.ac.uk
Dave Smith[3]
Dave.Smith@abm-tr.wales.nhs.uk

[1] Department of Computer Science
Swansea University, UK
[2] College of Engineering
Swansea University, UK
[3] ABM University NHS Trust
Swansea, UK

Abstract

We present a shape prior based graph cut method which does not require user initialisation. The shape prior is generalised from multiple training shapes, rather than using singular templates as priors. Weighted directed graph construction is used to impose geometrical and smooth constraints learned from priors. The proposed cost function is built upon combining selective feature extractors. A SVM classifier is used to determine an optimal combination of features in the presence of various IVUS tissues and artefacts. Comparative analysis on manually labelled ground-truth shows superior performance of the proposed method compared to conventional graph cut methods.

1 Introduction

Intra-vascular Ultrasound (IVUS) imaging is a catheter-based technology, which assesses the severity and morphology of the coronary artery stenosis. The media-adventitia border represents the outer coronary arterial wall located between the media and adventitia. The media layer exhibits as a thin dark layer in ultrasound and has no distinctive feature. It is surrounded by fibrous connective tissues called adventitia. The media-adventitia border in IVUS is disrupted by various forms of artefacts such as acoustic shadow or reverberation which can be caused by catheter guide-wire or fatty and cholesterol materials deposit and fibrosis formed inside the artery. Fig. 1 gives an example of IVUS image.

Common approaches to IVUS segmentation include graph cut and deformable modelling, and usually requires user initialisations [3, 7, 12]. The use of shape prior has shown to be a promising approach to tackle the ambiguities in identifying media-adventitia border. For example, Unal *et al.* [13] used principal component analysis (PCA) to generalise the shape variation. The initialisation of the media-adventitia border is based on the maximum

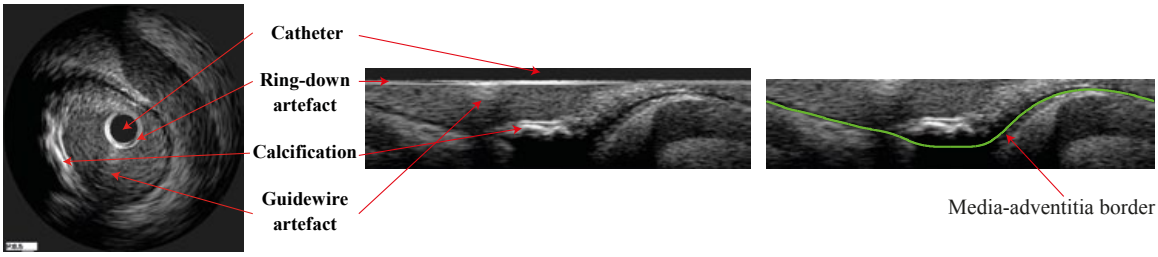

Figure 1: Pre-Processing steps. (a) Original IVUS image. (b) Polar transformed image. (c) After removing the catheter region.

intensities which can be distracted by fibrotic tissue and other imaging artefacts especially in high frequency ultrasound images.

The integration of shape prior into graph-based methods is still a challenging problem. Freedman and Zhang [6] defined the shape template as a distance function and embedded the average distance between every pair of pixels into the neighbourhood edges in the graph. However, this method effectively requires the user to place landmarks to define the initial shape. In [9], the authors proposed an iterative graph cut method. Kernel PCA was used to build the shape model. Affine transformation of shapes was not taken into account, and user initialisation is necessary.

In this paper, we propose an efficient graph cut algorithm to segment media-adventitia border in IVUS images without user initialisation. Prior knowledge of the IVUS tissue type is used to optimise the cost function. Weighted directed graph is defined to impose geometric constraints. The proposed method can handle large variations in training shapes which may undergo affine transformations. The generalised shape prior is incorporated in the cost function, as well as in the graph construction.

2 Proposed Method

The images are first transformed from Cartesian coordinates to polar coordinates and the catheter regions are removed (see Fig. 1). This transformation not only facilitates our feature extraction and classification but also transfers a closed contour segmentation to a "height-field" segmentation. The border to be extracted intersects once and once only with each column of pixels. This particular form of segmentation allows us to construct a node-weighted directed graph, on which a minimum path can be found without any user initialisation.

2.1 Feature extraction and classification

The imaging artifacts generally have large responses to image gradient based feature extraction. In this work, we propose to detect those artifacts and treat them differently when incorporating into the cost function. To highlight the media-adventitia border, we use a combination of derivative of Gaussian (DoG) features and local phase features. A set of first and second order DoG filters are applied to enhance the intensity difference between media and adventitia. Local phase [10] has shown to be effective in suppressing speckles in ultrasound images. We use the dark symmetry feature to highlight bar-like image patterns, which are useful to detect the thin media layer.

For those parts of media-adventitia border that are beneath various forms of image artifacts, such as calcification, their image features are suppressed by those artifacts. Hence, it is desirable to detect those artifacts and treat those columns of pixels differently to others.

Instead of a usual attempt of localising those image artifacts based on intensity profile, e.g. [5, 13], which is problematic, we classify entire columns of pixels that contain those image artifacts. The detection result will then have an influence on the formulation of the cost function. To this end, we train a SVM classifier to classify individual columns of pixels in the polar coordinates into one of the following five categories: calcification, fibrous plaque, stent, guide-wire artifact, and normal tissue or soft plaque.

2.2 Boundary based cost function

The boundary based energy term can be expressed as $E_B = \sum_{V \in S} \hat{c}_B(x,y)$, where $\hat{c}_B$ denotes the normalised cost function ($\hat{c}_B(x,y) \in [0,1]$) and S is a path in the directed graph. The formulation of the pre-normalisation cost function, c_B, is determined by the SVM classification result as presented below.

For normal tissue (or soft plaque), the media layer has a good contrast to adventitia. Hence, c_B is defined as $c_B(x,y) = D_1(x,y) - D_2(x,y)$ where D_1 is a summation of raw filtering response of the first order DoG at four different orientations and D_2 denotes maximum response of second order DoG filtering from different orientations across three scales. invariant measurement of bar-like feature.

Calcified plaque exhibits strong edge features and casts varying degree of acoustic shadow. Thus, we use the second order DoG responses to suppress calcification and enhance possible media layer. Fibrous tissue behaves similarly to calcification, except in majority cases media-adventitia border is still discernible. Hence, bar feature detection is more appropriate and to enhance the effect we combine it with phase symmetry feature, i.e. $c_B(x,y) = -D_2(x,y) - FS(x,y)$ where FS is the local phase feature.

The cost for stent case is the second order DoG responses with more weight underneath the stent region. For guide-wire artifact, we do not extract any feature and a positive constant is used as their cost value, since it is a small area and cast acoustic shadowing.

2.3 Shape prior based cost function

The energy term for shape prior can be expressed as:

$$E_S = \sum_{V \in S} c_S(x,y) + \sum_{(p,q) \in \mathcal{N}} f_{p,q}(S(p) - S(q)), \tag{1}$$

where c_S denotes the cost function associated to prior and f is a convex function penalizing abrupt changes in S between neighbouring columns p and q in the set $\mathcal{N}$ of neighbouring columns in the graph. The second term is realized through graph construction, detailed in the following Section 2.4.

Each shape in the training set is treated as a binary template, ψ where the area inside shape is one and the outside area is zero. The distance between two templates ψ^a and ψ^b is defined using a discrete version of Zhu and Chan distance [4]: $d^2(\psi^a, \psi^b) = \sum_P (\psi^a - \psi^b)^2$, where P denotes the image domain. This distance measure is a true metric and is not influenced by image size. Affine transformation is also applied to remove the influence from geometrical transformation. Let $\Psi = \psi^1, ..., \psi^N$ denote the N number of aligned shapes from the training set. Given a possible cut in the graph which produces an aligned binary shape f, its similarity to a shape template ψ^n in the training set is computed as $\alpha(f, \psi^n) = exp(-\frac{1}{2\sigma^2} d^2(f, \psi^n))$. Thus, the likelihood of this particular cut can be evaluated by taking into account of all training shapes: $\omega_s = \sum_{n=1}^{N} \alpha(f, \psi^n)\psi^n / \sum_{n=1}^{N} \alpha(f, \psi^n)$. The labelling of the shape likelihood and initial cut needs to be compared in order to assign appropriate

terminal arcs. For simplicity and efficiency, we search the lower bound of the likelihood function in the image domain and assign negative cost to this lower bound whileas other regions are assigned positive cost to form our shape cost term, c_S. Hence, we eliminate the need to identify the terminal connection type.

2.4 Graph construction using shape prior

Conventional graph cut, such as [1], generally requires user initialisation. In [8], Li *et al.* introduced a graph construction method which transforms surface segmentation in 3D into computing a minimum closed set in a directed graph without any user initialisation. Very recently, Song *et al.* [11] extended the method to incorporate shape prior by assuming that the relationship between every neighbouring columns can be represented by a parametric normal distribution. In this work, we propose an extension of this method by performing affine transformation based alignment of the training shapes and the use of a shape similarity metric in computing the inter-column parametric distribution. Additonally, we alter the inter-column arcs to permit more influence from the boundary features.

Let $G = \langle V, E \rangle$ denote the graph, where each node $V(x,y)$ corresponds to a pixel in the transformed IVUS image $I(x,y)$ in polar coordinates. The graph G consists of two arc types: intra-column arcs and inter-column arcs. For intra-column, along each column every node $V(x,y)$, where $y > 0$, has a directed arc to the node $V(x,y-1)$ with $+\infty$ weight assigned to the arc to ensure that the desired interface intersects with each column exactly once. Inter-column acts as a hard constraint and derived from shape prior. In calculating the shape prior cost function, an initial cut is first obtained by minimising the boundary based cost function alone. Note, this is fully automatic and there is no need for user initialisation. The training shapes are then affine-aligned to our initial graph cut. The similarity measurement α is used to choose a set of closest templates. The inter-column changes are then generalised using mean $m_{p,q}$ and standard deviation $\sigma_{p,q}$ at individual column. These statistics are then used in determining maximum and minimum distances when connecting neighbouring columns in graph construction, i.e. $\bar{\Delta}_{p,q} = m_{p,q} + c \cdot \sigma_{p,q}$, $\underline{\Delta}_{p,q} = m_{p,q} - c \cdot \sigma_{p,q}$, and c is a real constant.

Additional inter-column arcs are necessary in order to allow smooth transition. That is intermediate values, $h \in [\underline{\Delta}_{p,q}, \bar{\Delta}_{p,q}]$, are used to construct inter-column arcs. The direction of these arcs is based on the first order derivative of the function $f_{p,q}(h)$ as in (1). Here, we employ a quadratic function, $f_{p,q} = \lambda(x - m_{p,q})^2$, where λ is a weighting factor for smoothness constraint. If $f'_{p,q}(h) \geq 0$ an arc from $V(x,y)$ to $V(x+1, y-h)$ is established; otherwise, the arc is connected from $V(x+1,y)$ to $V(x,y+h)$. The weight for these arcs is assigned as the second order derivative of $f_{p,q}$ for the intermediate values of h, and $+\infty$ weight for the endpoints of the interval. Note, when $f'_{p,q}(h) = 0$, only single arc is defined to reduce the shape prior influence in presence of strong boundary features, instead of using bi-directional arcs on the mean difference $m_{p,q}$.

2.5 Compute the minimum closed set

The cost function $C(x,y) = c_B(x,y) + c_S(x,y)$ is inversely related to the likelihood that the border of interest passes through pixel (x,y). The weight for each node on the directed graph can be assigned as:

$$w(x,y) = \begin{cases} C(x,y) & \text{if } y = 0, \\ C(x,y) - C(x,y-1) & \text{otherwise.} \end{cases} \tag{2}$$

Segmenting the media-adventitia is equivalent to finding the minimum closed set in the directed graph. The *s-t* cut algorithm [2] can then be used to find the minimum closed

Table 1: Quantitative comparison to $s-t$ cut. AD: area difference in percentage; AMD: absolute mean difference in pixel in comparison to groundtruth.

	$s-t$ cut		proposed method	
	AD	AMD	AD	AMD
Mean	22.54	23.91	8.71	9.46
Std.	8.87	7.49	4.99	5.36

set, based on the fact that the weight can be used as the base for dividing the nodes into nonnegative and negative sets. The source s is connected to each negative node and every nonnegative node is connected to the sink t, both through a directed arc that carries the absolute value of the cost node itself. The segmented media-adventitia may still contain local oscillations. Here, efficient 1D RBF interpolation using thin plate base function is used to obtain the final interface.

3 Experimental results

A total of 1197 IVUS images of 240×1507 pixels in the polar coordinates from 4 pullbacks acquired by a 40 MHz transducer are used to evaluate the proposed method. These images contain various forms of fibrous plaque, calcification, stent, and acoustic shadow. For all the tested images, ground-truth via manual labelling is available for quantitative analysis. The training shape set contains 278 images. Another set of 138 images are used to train SVM classifier.

First, we compared our method against the $s-t$ cut algorithm [1]. Despite reasonable care in initialisation as shown Fig. 2(a), the $s-t$ cut result was not satisfactory. The corresponding results of the proposed method are shown in the second column. The bottom of the each image shows the classification result of detecting different types of tissue. The proposed method achieved better accuracy and consistency. The quantitative comparison was carried out on a randomly selected subset of 50 images, since manual initialisation of 1197 images is too labour intensive. Table 1 shows that the proposed method clearly outperformed $s-t$ cut in both area difference measure (AD) and absolute mean difference measure (AMD) based on groundtruth. Next, the proposed method was tested on the full dataset (1197 images) and its performance based on labelled groundtruth can be summarised as: 7.88% mean AD with standard deviation of 5.79 and 8.49 pixel mean AMD with standard deviation of 5.91. This is marginally better than the first subset. Fig. 3 shows example comparisons to groundtruth.

4 Conclusions

We presented an automatic graph based segmentation method for delineating the media-adventitia border in IVUS images. Boundary based features were dynamically selected to optimise the cost function. The use of multiple training shapes proved to be beneficial. The generalised shape prior was used in both incorporating the cost function but also graph construction. Qualitative and quantitative results on a large number of IVUS images showed superior performance of the method.

References

[1] Y. Boykov and G. Funka-Lea. Interactive graph cuts for optimal boundary and region segmentation of objects in n-d images. *IJCV*, 70(2):109–131, 2006.

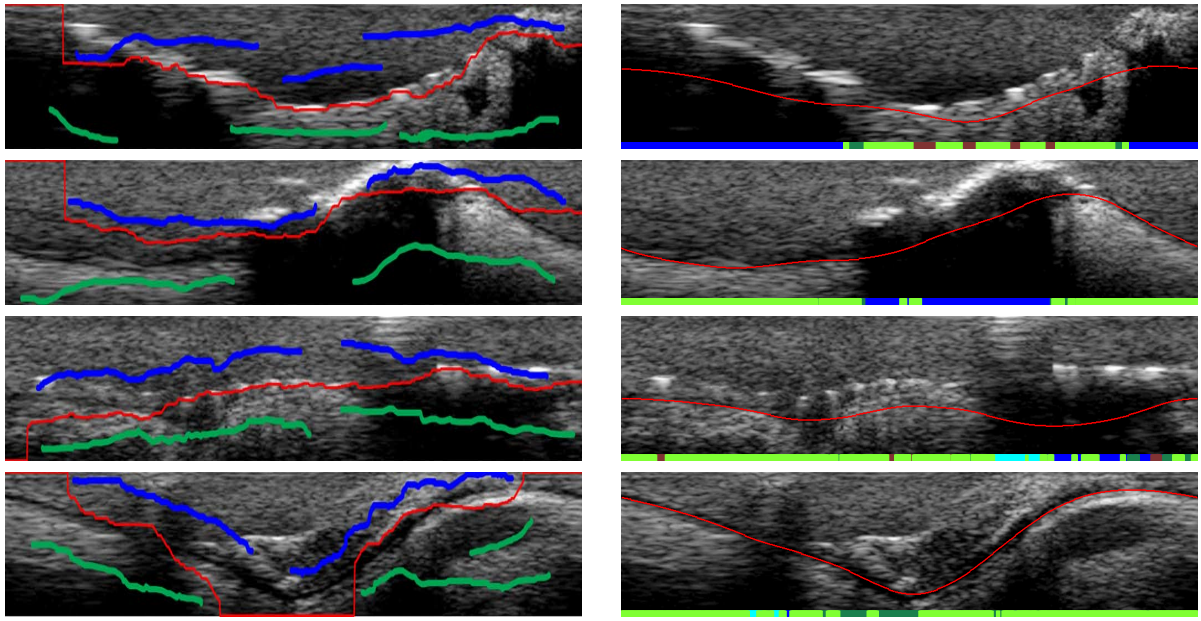

(a) (b)

Figure 2: (a) $s-t$ cut result (red) with user initialization (object: blue, background: green). (b) proposed method result; the bottom of each image also shows the classification result: calcified plaque (blue), fibrotic plaque (dark green), stent (dark red), guide-wire shadowing (cyan), and soft plaque/normal tissue (light green).

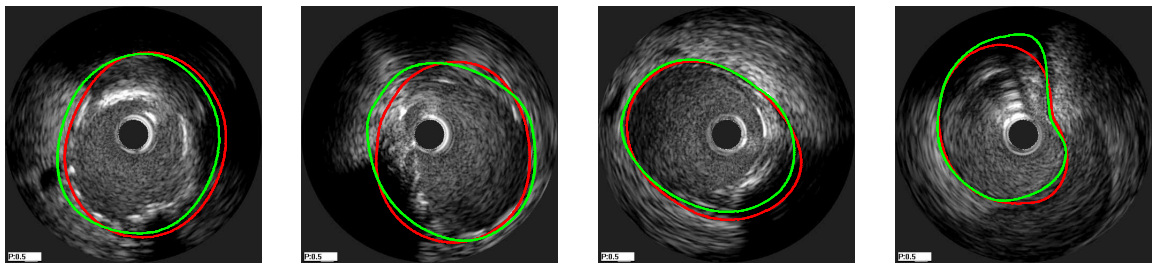

Figure 3: Comparison between groundtruth (green) and the proposed method (red).

[2] Y. Boykov and V. Kolmogorov. An experimental comparison of min-cut/max-flow algorithms for energy minimization in vision. *T-PAMI*, 26(9):1124–1137, 2004.

[3] M. R. Cardinal and et al. Intravascular ultrasound image segmentation: a three-dimensional fast-marching method based on gray level distributions. *T-MI*, 25(1):590–601, 2006.

[4] T. Chan and W. Zhu. Level set based shape prior segmentation. In *CVPR*, 2005.

[5] Esmeraldo Filho and et al. Detection & quantification of calcifications in ivus by automatic thresholding. *Ultrasound in Medicine and Biology*, 34(1):160–165, 2008.

[6] D. Freedman and T. Zhang. Interactive graph cut based segmentation with shape priors. In *CVPR*, pages 755–762, 2005.

[7] J. D. Klingensmith, R. Shekhar, and D. G. Vince. Evaluation of three-dimensional segmentation algorithms for the identification of luminal and medial adventitial borders in intravascular ultrasound images. *T-MI*, 19(10):996–1011, 2000.

[8] Kang Li, Xiaodong Wu, Danny Z. Chen, and Milan Sonka. Optimal surface segmentation in volumetric images-a graph theoretic approach. *T-PAMI*, 28(1):119–134, 2006.

[9] J. Malcolm, Y. Rathi, and A. Tannenbaum. Graph cut segmentation with nonlinear shape priors. In *ICIP*, pages 365–368, 2007.

[10] M. Mulet-Parada and J. Noble. 2D + T acoustic boundary detection in echocardiography. *MIA*, 4 (1):21–30, 2000.

[11] Qi Song, Xiaodong Wu, Yunlong Liu, Mona Garvin, and Milan Sonk. Simultaneous searching of globally optimal interacting surfaces with shape priors. In *CVPR*, pages 2879–2886, 2010.

[12] Milan Sonka and et al. Segmentation of intravascular ultrasound images: A knowledge-based approach. *T-MI*, 14:719–732, 1995.

[13] Gozde Unal and et al. Shape-driven segmentation of the arterial wall in intravascular ultrasound images. *IEEE Trans. Info. Tech. in Biomed.*, 12(3):335–347, 2008.